Annals of Nuclear Energy 166 (2022) 108802

Contents lists available at ScienceDirect

Annals of Nuclear Energy

journal homepage: www.elsevier.com/locate/anucene

Dynamic characteristics of tube bundles with crack subjected to cross-flow and loose support

Jiang Lai [a,b,1,*], Lingling Lu [c,1], Shihao Yang [b], Tiancai Tan [b], Lei Sun [b]

[a] State Key Laboratory of Hydraulic Engineering Simulation and Safety, Tianjin University, China
[b] Nuclear Power Institute of China, Chengdu 610213, China
[c] Key Laboratory for Mechanics in Fluid Solid Coupling Systems, Chinese Academy of Sciences, Institute of Mechanics, Beijing 100190 China

ARTICLE INFO

Article history:
Received 14 September 2021
Received in revised form 18 October 2021
Accepted 2 November 2021
Available online xxxx

Keywords:
Flow-induced vibration
Tube bundles
Cross-flow
Crack
Dynamic response

ABSTRACT

Flow-induced vibration of the tube bundles subjected to cross-flow and loose support is an important issue in the security of a steam generator. In the operation of nuclear power station, the flow-induced vibration of the tube bundles may lead to crack initiation and propagation, which can affect the natural frequency and the dynamic response of the tube. However, there is seldom theoretical analysis to study the dynamic characteristics of cracked tube bundles subjected to cross-flow. Therefore, a mathematical model of a single cracked tube in a rotated triangular tube array subjected to cross-flow and loose support was presented in this paper. The model takes into account the variations of the tube natural frequency and mode of vibration owing to the crack damage. The effect of the crack damage on the dynamic characteristics of a flexible tube in tube bundles subject to cross-flow and loose support was investigated, and the dynamic responses of the cracked tube for three flow pitch velocity conditions were calculated.

1. Introduction

Flow-induced vibration of the tube bundles of a steam generator is a significant problem in nuclear industry. The vibration characteristics of the tubes may become very complicated, when the cross-flow velocity closes to the threshold of the fluidelastic instability of the tube array. Several experimental and theoretical studies were carried out to investigate the dynamic characteristics of the tube bundles for the past decades.

Tanaka and Takahara (1981) carried out several experiments to obtain the unsteady fluid force acting on a cylinder in cross-flow. By using the measured unsteady fluid force, the critical velocity of fluidelastic instability was calculated. Some experiments were performed to investigate the vibration behavior of a flexible tube within otherwise fixed tube bundles with different geometries by Austermann and Popp (1995). The experimental results indicated that the array pattern and tube distance had an obvious effect on the threshold of fluidelastic instability. Series of experiments were carried out to measure the motion-dependent fluid force coefficients by Chen and Srikantiah (2001). Based on the unsteady flow theory, the fluid damping and stiffness coefficients were obtained as a function of excitation amplitude, reduced flow velocity, and Reynolds number.

The existence of gaps between the tube and support structure has a great influence on the flow-induced vibration of the heat exchanger tube bundles. Thus, Hassan and Hayder (2008) presented a time-domain model to study the fluidelastic instability of tube bundles with loose support. By using this model, the critical velocity, dynamic response, and impact force between the tube and support, which were sensitive to both the gap size and turbulence level, were calculated. Wang and Ni (2010) used an analytic model to investigate the Hopf bifurcation and chaotic motions of a cantilever tube impacting on a loose support. They found that the vibration amplitude of the tube grows with increasing of the flow velocity. The collision between the tube and support may lead to some complex motions, such as chaos and quasi-periodic motions for a high flow velocity. Zhao *et al.* used a fully coupled model to calculate the dynamic responses of tube bundles subjected to cross-flow. Then, the time trace, power spectral density, phase-plane plot and Poincaré map were used to analyze the tube motion (Zhao et al., 2014). Zhang et al. (2016) carried out an experiment to study the fluidelastic instability of a rigid parallel triangular tube array considering the effects of increasing and decreasing flow velocities. The nonlinear hysteresis phenomenon was observed in the experiment. Li and Mureithi presented a new time delay formulation for the quasi-steady model, which is dependent on the Reynolds number, to predict the threshold of the fluidelastic insta-

* Corresponding author at: Nuclear Power Institute of China, Chengdu 610213, China.
E-mail address: laijiang1983@163.com (J. Lai).
[1] These authors equally contributed to this work.

https://doi.org/10.1016/j.anucene.2021.108802
0306-4549/

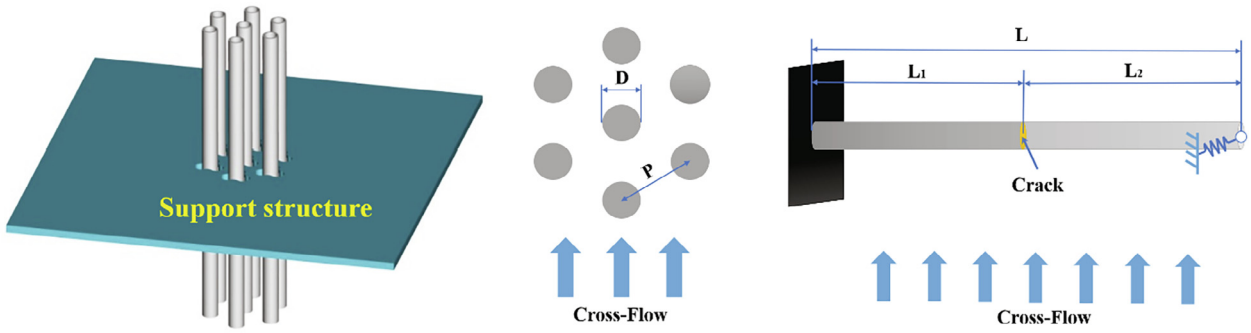

Fig. 1. The schematic of tube bundles with a crack subject to cross-flow and loose support.

bility of tube bundles. The numerical results indicated a significant improvement over the constant time delay quasi-steady model the quasi-unsteady model (Li and Mureithi, 2017).

Some CFD calculations have be carried out to obtain the fluid force acting the tube bundles. Based on the RANS formulation with aid of Spalart-Allmaras turbulentce model, Sadek et al. (2018) presented a numerical model to obtain the unsteady fluid forces of two-phase flow acting on a parallel triangular tube array. The comparison between the numerical and experimental results showed a good agreement. de Pedro Palomar and Meskell (2018) presented a steady RANS simulation to obtain the static fluid forces acting on a normal triangular tube array. With these fluid forces, the critical velocity of tube bundle was obtained. Piteau et al. (2019) carried out several experiments to obtain the fluidelastic coupling forces on a flexible tube in a rigid square bundle subjected to single-phase cross-flow. Their experimental results indicated that the formulations for coefficient reduction may be improved. Xu et al. (2019) performed a series of experimental studies on flow-induced vibration of two identical elastically mounted circular cylinders in tandem arrangement in a low turbulence surface water channel.

In our previously reported papers, a series of experiments were carried out to obtain the thresholds of the fluidelastic instability of a rotated triangular tube array subjected to two-phase flow both in the transverse and parallel directions (Lai et al., 2019; Lai, 2019; Lai et al., 2020). Considering the effect of two-phase flow, two theoretical models (Lai et al., 2019; Lai et al., 2020) of the tube bundles to predict the critical velocity of the fluidelastic instability of tube bundles in the transverse and parallel direction were presented, respectively. Based on these theoretical models, the two-phase flow-induced instability and nonlinear dynamics of the tube bundles subjected to two-phase flow and loose support were investigated (Lai et al., 2019; Lai et al., 2020; Lai et al., 2020). These investigations demonstrate that the natural frequency of the tube is a significant parameter to the fluidelastic instability and dynamic response of the tube bundles.

As mentioned above, several experimental and numerical studies of the fluidelastic instability and dynamic response of the tube bundles subjected to cross-flow have been performed with intact tube bundles models. However, in the operation of nuclear power station, the flow-induced vibration of the tube bundles in the steam generator may lead to crack initiation and propagation. It is important to note that the presence of a crack cannot only change the natural frequency of the structure, but it can affect the dynamic response of the structure (Ostachowicz and Krawczuk, 1991; Chati et al., 1997). Thus, after considering the effects of a crack, how the dynamic response of the tube bundles will change, which is worthy of further study.

In the present work, a theoretical model of a flexible tube with a crack in tube bundles was presented. Based on this model, the dynamic responses of the cracked tube were obtained, and the dynamic characteristics of the cracked tube were also investigated. In the work, we have focused on the study of dynamic characteristics of the cracked tube in the transverse direction.

2. Theoretical analysis

A model of a single flexible tube in tube bundles subject to cross-flow considering the effect of tube support plate was illustrated in Fig. 1. The motion equation for the flexible tube can be expressed as:

$$EI\frac{\partial^4 w(y,t)}{\partial y^4}+c_t\frac{\partial w(y,t)}{\partial t}+m_t\frac{\partial^2 w(y,t)}{\partial t^2} = \delta(y-y_a)F_{stiffness}(w)+F_{unsteady}(w,\dot{w},\ddot{w}) \quad (1)$$

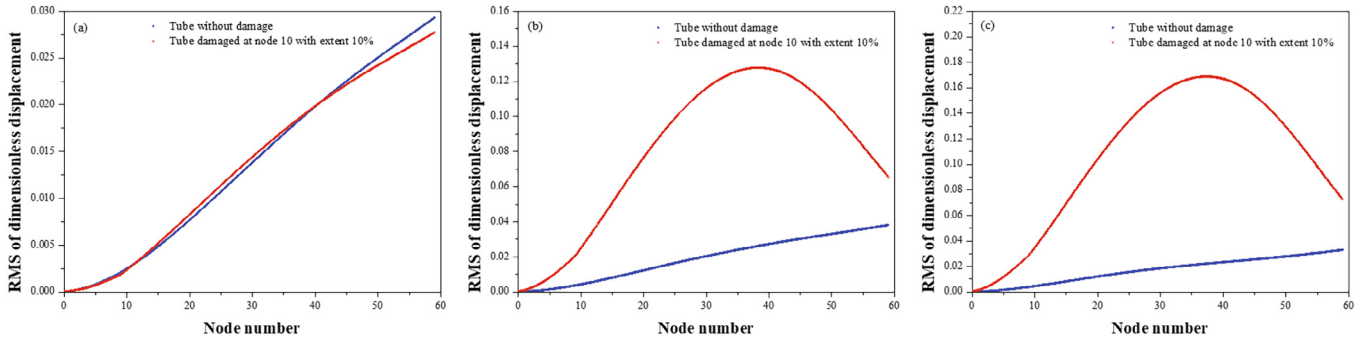

Fig. 2. The comparison of the RMS of dimensionless displacements the tube: (a) Flow pitch velocity is 1.476 m/s; (b) Flow pitch velocity is 1.938 m/s; (c) Flow pitch velocity is 2.399 m/s.

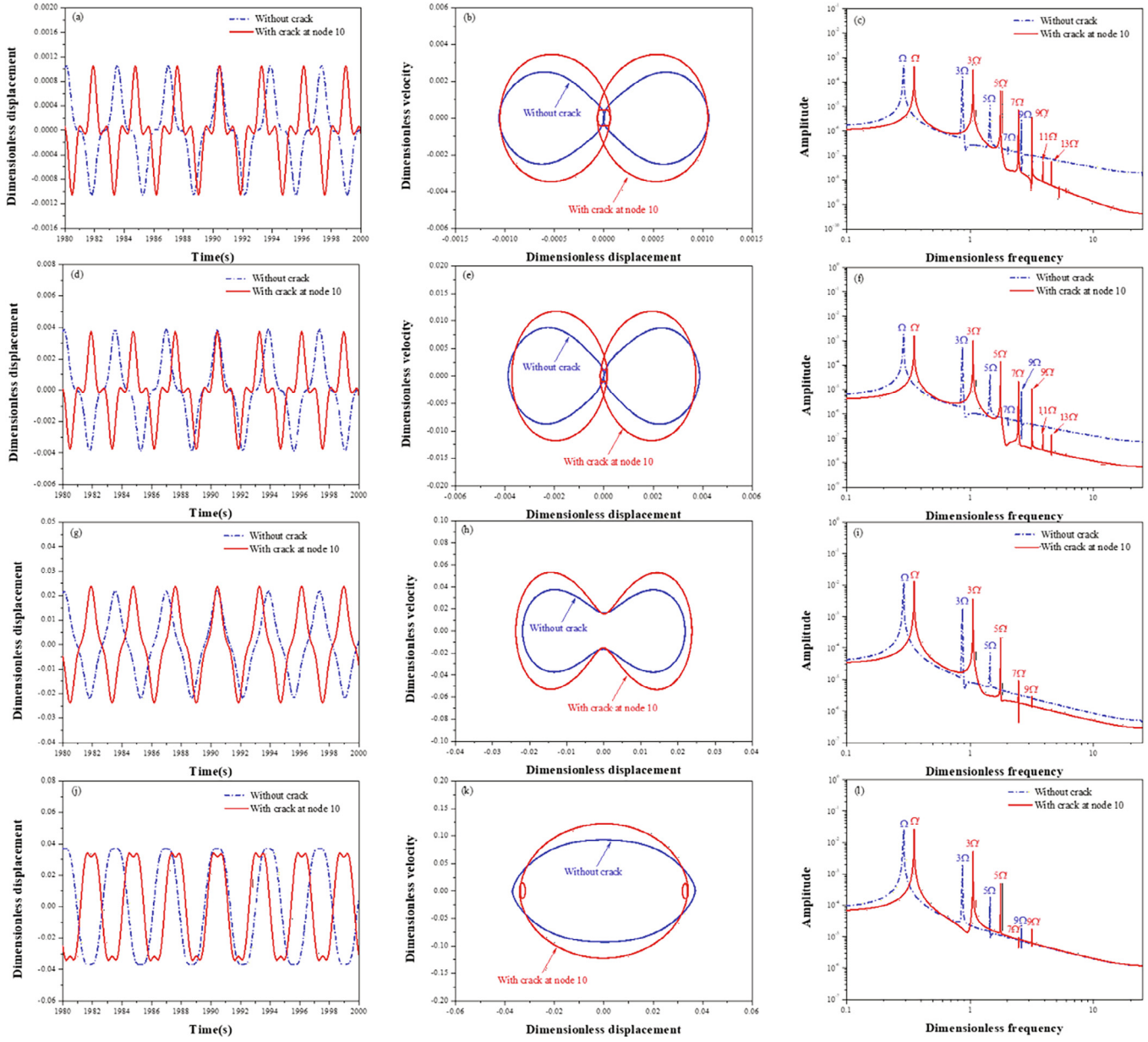

Fig. 3. The comparison of the dimensionless displacements, limit cycles and dimensionless frequency spectrum of the tube when the flow pitch velocity is 1.476 m/s: (a)(b)(c) Node 5; (d)(e)(f) Node 10; (g) (h)(i) Node 30; (j)(k)(l) Node 60.

where EI is the rigidity modulus of the tube, w is lateral displacement of the tube, c_t, m_t and m_a is the damping coefficient, the mass and the added mass of the tube per unit length, $\delta(y\text{-}y_a)$ is the Dirac delta function, $F_{stiffness}(w)$ is the impact force between the tube and support structure, $F_{unsteady}(w, \dot{w}, \ddot{w})$ is the fluid force of the cross-flow, where dot and double dot indicate the velocity and acceleration of the tube, respectively.

An unsteady fluid force model can be used to predict the threshold of fluidelastic instability of a rotated triangular tube array in cross-flow. And, $F_{unsteady}(w, \dot{w})$ can be expressed as:

$$F_{unsteady}(w,\dot{w},\ddot{w}) = m_a\frac{\partial^2 w(y,t)}{\partial t^2} + c_a\frac{\partial w(y,t)}{\partial t} + k_a w(y,t) \tag{2}$$

where, the added mass, m_a, added damping, c_a, and added stiffness, k_a, can be written as:

$$\begin{aligned} m_a &= \frac{\pi}{4}\rho D^2\left[\frac{(D_e/D)^2+1}{(D_e/D)^2-1}\right] \\ c_a &= \frac{\rho U_\infty^2 C_F \cos\Phi_F}{2} \\ k_a &= \frac{\rho U_\infty^2 C_F \sin\Phi_F}{2\omega} - \omega^2 m_a \end{aligned} \tag{3}$$

where ρ is the cross-flow density, respectively, D, D_e is the tube diameter and pitch between tube bundles, respectively, U_∞ is the free stream velocity, ω is the angular frequency of the tube, C_F, Φ_F is the unsteady fluid force coefficient magnitude and phase which can be obtained from the experimental study presented by Sawadogo and Mureithi (2014).

The flow pitch velocity in the tube bundles can be calculated from the free stream velocity, U_∞, as:

$$U_p = \frac{P}{P-D}U_\infty \tag{4}$$

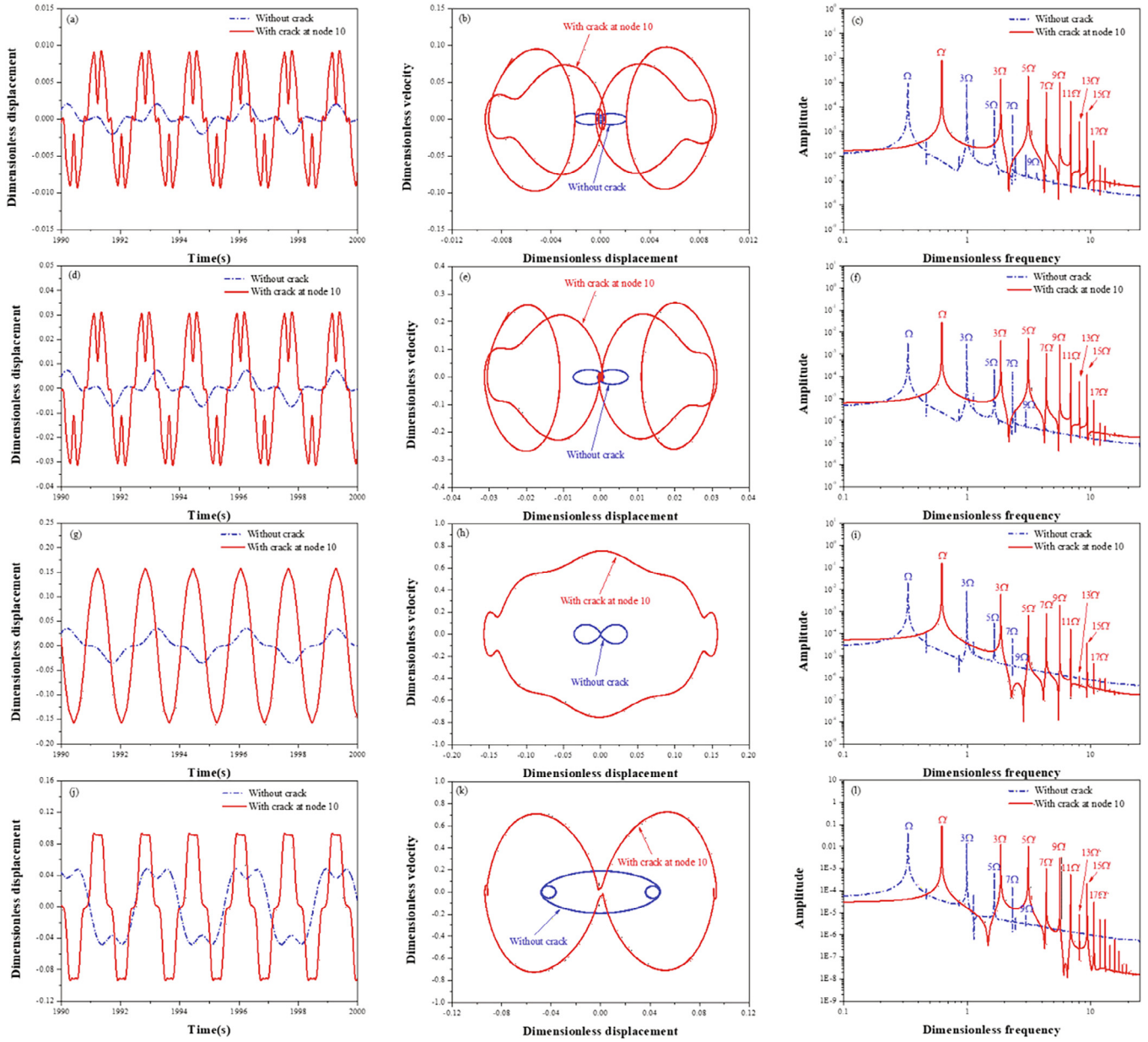

Fig. 4. The comparison of the dimensionless displacements, limit cycles and dimensionless frequency spectrum of the tube when the flow pitch velocity is 1.938 m/s: (a)(b)(c) Node 5; (d)(e)(f) Node 10; (g)(h)(i) Node 30; (j)(k)(l) Node 60.

Moving the flow force of the cross-flow to the left-hand side in equation as forms of contribution to the mass, damping, and stiffness, the general form of the coupling equation can be obtained.

Introducing the following non-dimensional quantities:

$$\eta=\frac{w}{D},\quad \xi=\frac{y}{L},\quad \tau=\lambda_1^2\sqrt{\frac{EI}{m_t L^4}}t=\Omega t,\quad \varsigma=\frac{c_t}{\Omega m_t},$$
$$m^*=\frac{m_t}{\rho D^2},\quad U^*=\frac{2\pi U_\infty}{D\Omega},\qquad (5)$$
$$\alpha=\frac{1}{1+4m^*/(\pi C_{ma})},\quad \omega^*=\frac{\omega}{\Omega}$$

where L is the tube length, λ_1 is the dimensionless eigenvalue of the first-order mode for a cantilever tube.

Substituting these dimensionless quantities into equation (1), the partial differential equation of the motion of the tube bundles subject to cross-flow and loose support can be rewritten as:

$$\frac{1}{1-\alpha}\frac{\partial^2\eta}{\partial\tau^2}(\xi,\tau)+\left[\varsigma-\frac{U^{*2}C_F\sin\Phi_F}{8\pi^2 m^*\omega^*}\right]\frac{\partial\eta}{\partial\tau}(\xi,\tau)+\frac{1}{\lambda_1^4}\frac{\partial^4\eta}{\partial\varsigma^4}(\xi,\tau)$$
$$-\left[\frac{U^{*2}C_F\cos\Phi_F}{8\pi^2 m^*}-\frac{\alpha\omega^{*2}}{1-\alpha}\right]\eta(\xi,\tau)+\delta(\xi-\xi_b)f^*(\eta)=0 \qquad (6)$$

With a crack damage, the tube was divided into two parts with the same section properties, as shown in Fig. 1. Thus, the dimensionless displacement of the tube with a crack can be expressed as:

$$\eta(\xi,\tau)=\begin{cases}\sum_{i=1}^{N_1}\varphi_{1i}(\xi)q_i(\tau) & -L_1\leqslant x<0^-\\ \sum_{i=1}^{N_2}\varphi_{2i}(\xi)q_i(\tau) & 0^+\leqslant x<L_2\end{cases} \qquad (7)$$

The mode shape function of each part can be written as:

$$\varphi_{1i}(x)=C_{11}\cosh\lambda_i x+C_{12}\sinh\lambda_i x+C_{13}\cos\lambda_i x+C_{14}\sin\lambda_i x L_1\leqslant x<0^-$$
$$\varphi_{2i}(x)=C_{21}\cosh\lambda_i x+C_{22}\sinh\lambda_i x+C_{23}\cos\lambda_i x+C_{24}\sin\lambda_i x 0^+\leqslant x<L_2 \qquad (8)$$

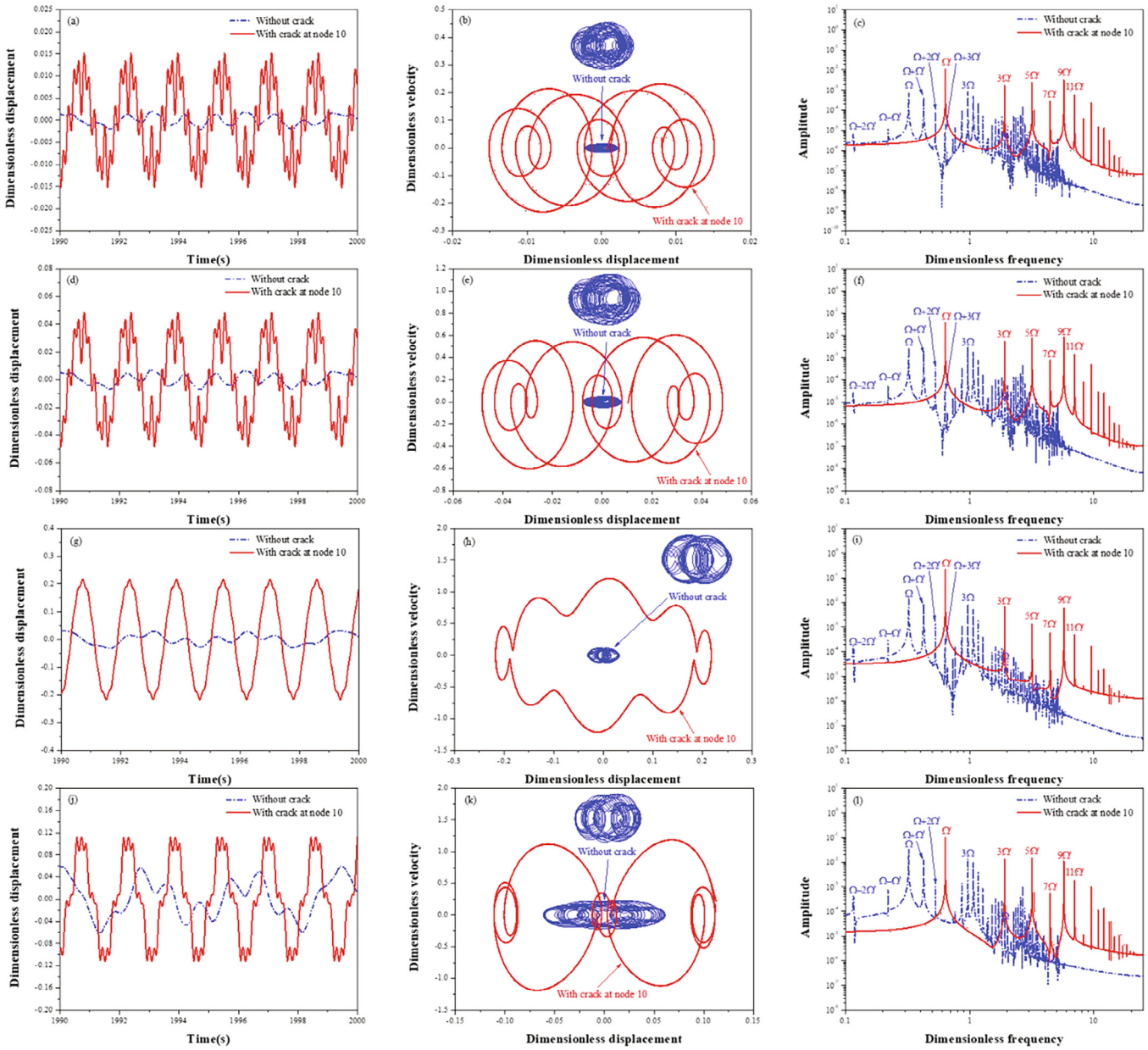

Fig. 5. The comparison of the dimensionless displacements and limit cycles of the tube when the flow pitch velocity is 2.399 m/s: (a) (b) (c) Node 5; (d) (e) (f) Node 10; (g) (h) (i) Node 30; (j)(k)(l) Node 60.

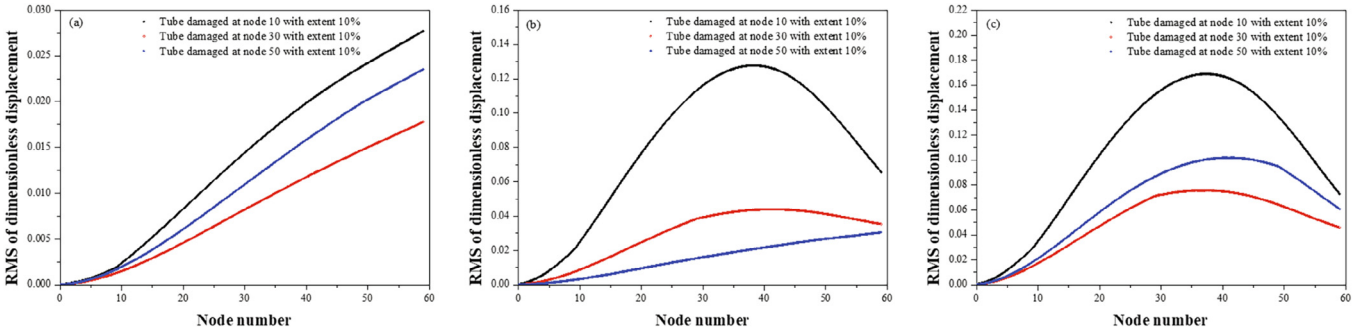

Fig. 6. The comparison of the RMS of dimensionless displacements the tube: (a) The flow pitch velocity is 1.476 m/s; (b) The flow pitch velocity is 1.938 m/s; (c) The flow pitch velocity is 2.399 m/s.

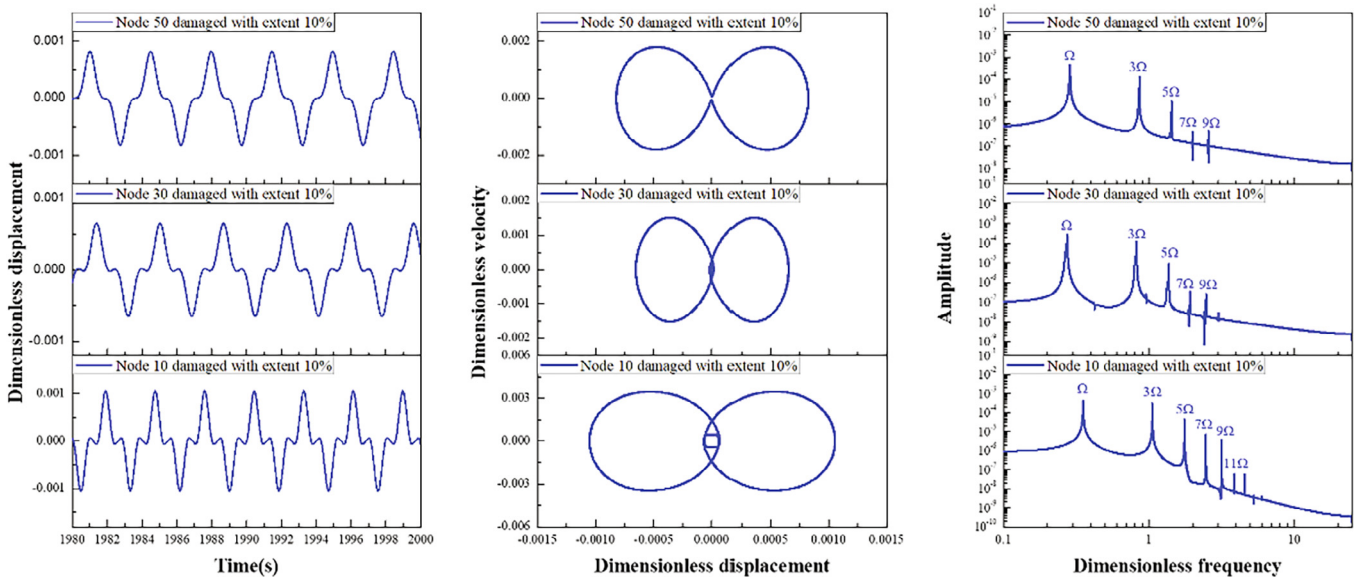

Fig. 7. The comparison of the dimensionless displacements and limit cycles of the node 5 of the tube when the flow pitch velocity is 1.476 m/s.

The corresponding boundary conditions of the two parts are as follows:

$$
\begin{aligned}
&x = -L_1 : \begin{cases} \varphi_{1i}(-L_1) = 0 \\ \varphi'_{1i}(-L_1) = 0 \end{cases} \\
&x = L_2 : \begin{cases} \varphi''_{2i}(L_2) = 0 \\ \varphi'''_{2i}(L_2) = 0 \end{cases} \\
&x = 0 : \begin{cases} \varphi_{1i}(0^-) = \varphi_{2i}(0^+) \\ \varphi''_{1i}(0^-) = \varphi''_{2i}(0^+) \\ \varphi'''_{1i}(0^-) = \varphi'''_{2i}(0^+) \\ -EI\varphi''_{1i}(0^-) = K_T[\varphi'_{1i}(0^-) - \varphi'_{2i}(0^+)] \end{cases}
\end{aligned} \tag{9}
$$

where L_1 is the length of the left part of the tube, L_2 is the length of the right part of the tube, K_T is the rigidity modulus of the tube at the crack damage position which can be obtained from reference (Bamnios and Trochides, 1995).

Substituting equation into equation, the frequency equation of the tube with a crack can be obtained as follows:

$$
\begin{aligned}
&2\frac{K_T}{EI\lambda_i} + 2\frac{K_T}{EI\lambda_i}\cos\lambda_i(L_1+L_2) \times \cosh\lambda_i(L_1+L_2) + \cosh\lambda_i L_1 \times \sin\lambda_i L_1 \\
&- \cosh\lambda_i L_2 \times \sin\lambda_i L_2 - \sin\lambda_i(L_1+L_2) \times \cosh\lambda_i L_1 \times \cosh\lambda_i L_2 \\
&- \cos\lambda_i L_1 \times \sinh\lambda_i L_1 + \cos\lambda_i L_2 \times \sinh\lambda_i L_2 + \sinh\lambda_i(L_1+L_2) \\
&\times \cos\lambda_i L_1 \times \cos\lambda_i L_2 = 0
\end{aligned} \tag{10}
$$

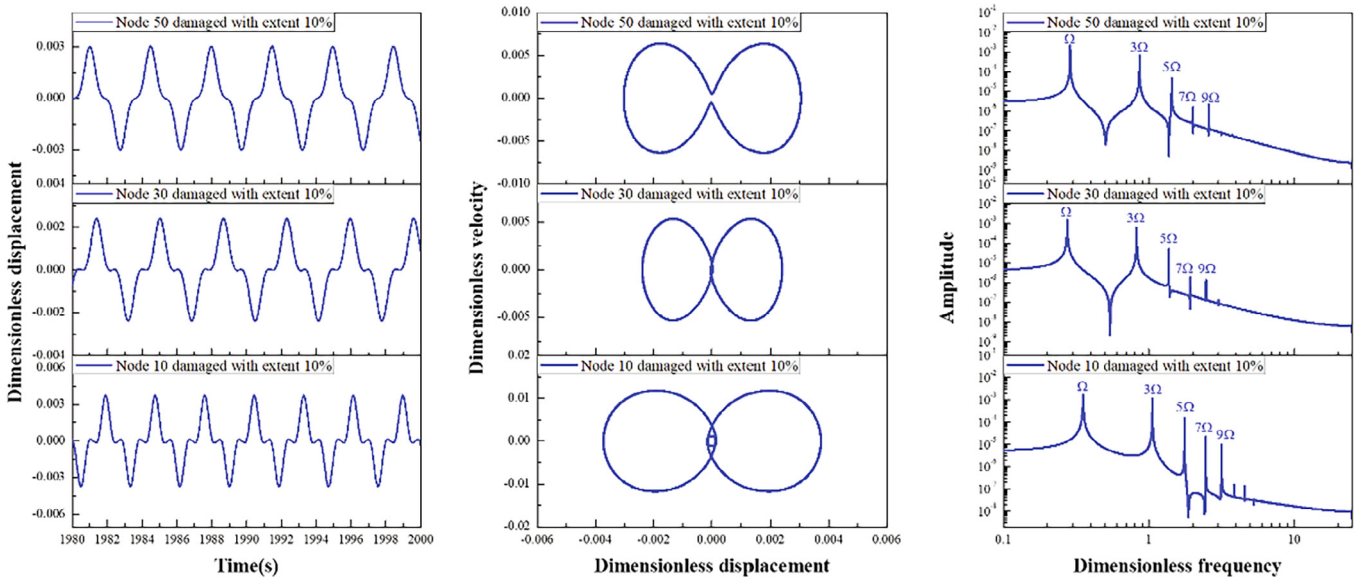

Fig. 8. The comparison of the dimensionless displacements and limit cycles of the node 10 of the tube when the flow pitch velocity is 1.476 m/s.

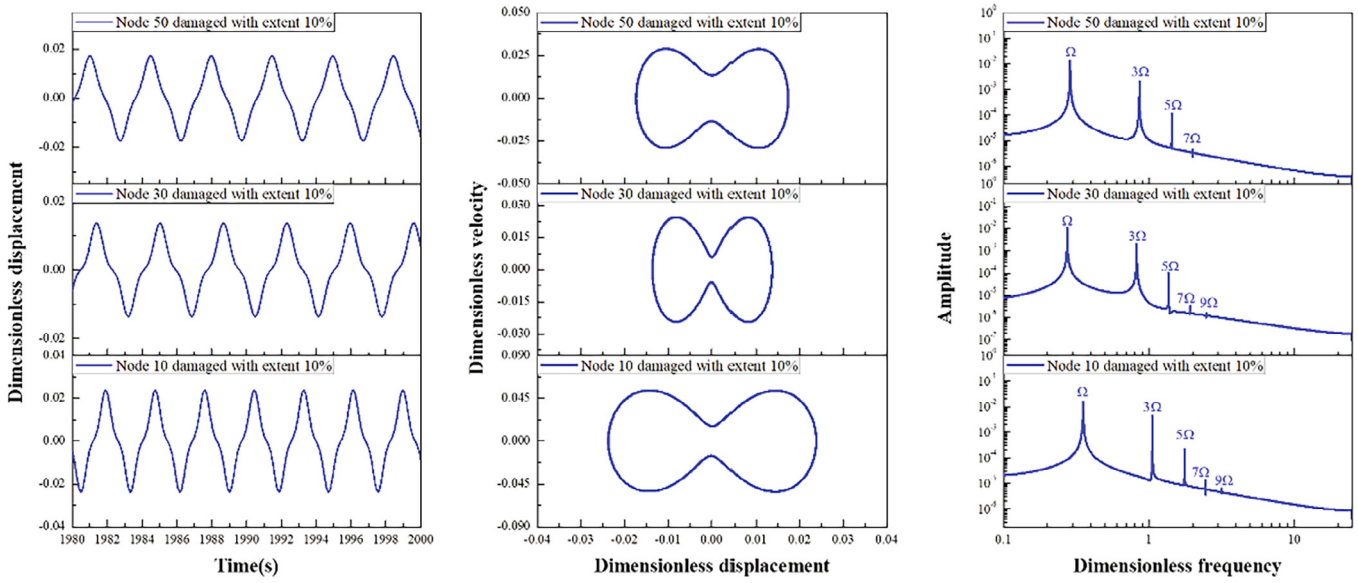

Fig. 9. The comparison of the dimensionless displacements and limit cycles of the node 30 of the tube when the flow pitch velocity is 1.476 m/s.

The mode shape functions of the tube with a crack, determined by boundary conditions, can be expressed as:

$$\varphi_{1i}(x) = \cosh\lambda_i x + \frac{C_{12}}{C_{11}}\sinh\lambda_i x + \frac{C_{13}}{C_{11}}\cos\lambda_i x + \frac{C_{14}}{C_{11}}\sin\lambda_i x$$
$$\varphi_{2i}(x) = \cosh\lambda_i x + \frac{C_{22}}{C_{11}}\sinh\lambda_i x + \frac{C_{13}}{C_{11}}\cos\lambda_i x + \frac{C_{24}}{C_{11}}\sin\lambda_i x \quad (11)$$

where, $\frac{C_{12}}{C_{11}}$, $\frac{C_{13}}{C_{11}}$, $\frac{C_{14}}{C_{11}}$, $\frac{C_{22}}{C_{11}}$, $\frac{C_{24}}{C_{11}}$ can be expressed as:

$$\frac{C_{12}}{C_{11}} = -\frac{(a_3b_4+a_4b_3)(a_1a_3-a_2a_4)-(a_1b_4-a_4b_1)(a_3a_3+a_4a_4)}{(a_3b_4+a_4b_3)(a_1a_4-a_2a_3)+(a_2b_4+a_4b_2)(a_3a_3+a_4a_4)}$$
$$\frac{C_{13}}{C_{11}} = -\frac{(a_1a_3-a_2a_4)(a_2b_4+a_4b_2)+(a_1a_4-a_2a_3)(a_1b_4-a_4b_1)}{(a_3a_3+a_4a_4)(a_2b_4+a_4b_2)+(a_1a_4-a_2a_3)(a_3b_4+a_4b_3)}$$
$$\frac{C_{14}}{C_{11}} = \frac{(a_1a_4+a_3a_2)(a_3b_2-a_2b_3)+(a_2a_4+a_3a_1)(a_1b_3+a_3b_1)}{(a_4a_4+a_3a_3)(a_3b_2-a_2b_3)+(a_2a_4+a_3a_1)(a_4b_3+a_3b_4)}$$
$$\frac{C_{22}}{C_{11}} = \frac{C_{12}}{C_{11}} + \frac{EI\lambda_i}{2K_T}\left(1-\frac{C_{13}}{C_{11}}\right)$$
$$\frac{C_{24}}{C_{11}} = \frac{C_{14}}{C_{11}} + \frac{EI\lambda_i}{2K_T}\left(1-\frac{C_{13}}{C_{11}}\right) \quad (12)$$

where,

$$a_1 = \cosh\lambda_i L_1, a_2 = \sinh\lambda_i L_1, a_3 = \cos\lambda_i L_1, a_4 = \sin\lambda_i L_1$$
$$b_1 = \cosh\lambda_i L_2 + \frac{EI\lambda_i}{2K_T}\sinh\lambda_i L_2 - \frac{EI\lambda_i}{2K_T}\sin\lambda_i L_2, b_2 = \sinh\lambda_i L_2$$
$$b_3 = \cos\lambda_i L_2 + \frac{EI\lambda_i}{2K_T}\sinh\lambda_i L_2 - \frac{EI\lambda_i}{2K_T}\sin\lambda_i L_2, b_4 = \sin\lambda_i L_2 \quad (13)$$
$$d_1 = \sinh\lambda_i L_2 + \frac{EI\lambda_i}{2K_T}\cosh\lambda_i L_2 - \frac{EI\lambda_i}{2K_T}\cos\lambda_i L_2, d_2 = \cosh\lambda_i L_2$$
$$d_3 = \sin\lambda_i L_2 - \frac{EI\lambda_i}{2K_T}\cosh\lambda_i L_2 + \frac{EI\lambda_i}{2K_T}\cos\lambda_i L_2, d_4 = \cos\lambda_i L_2$$

It is known that the dynamic response of a tube is dominated by the first low modes. Thus, the first five order modes were chosen in present study.

Then, a set of ordinary differential equations can be deduced from the partial differential equation, as follows:

$$\frac{\ddot{q}_i}{1-\alpha} + \left(\zeta - \frac{U^{*2}C_F\sin\Phi_F}{8\pi^2 m^*\omega^*}\right)\dot{q}_i + \left(\frac{\lambda_i^4}{\lambda_1^4} - \frac{U^{*2}C_F\cos\Phi_F}{8\pi^2 m^*} + \frac{\alpha\omega^{*2}}{1-\alpha}\right)q_i + f^*(\eta_a)\varphi_i(\xi_a) = 0 (i = 1,2,3,4,5) \quad (14)$$

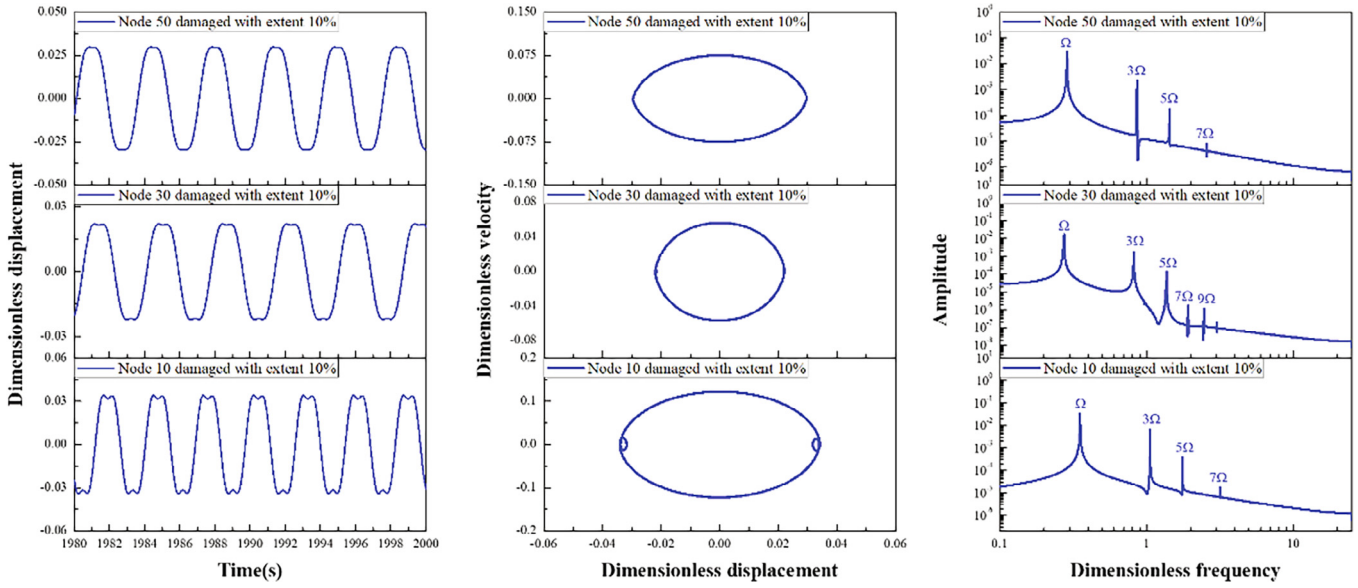

Fig. 10. The comparison of the dimensionless displacements and limit cycles of the node 60 of the tube when the flow pitch velocity is 1.476 m/s.

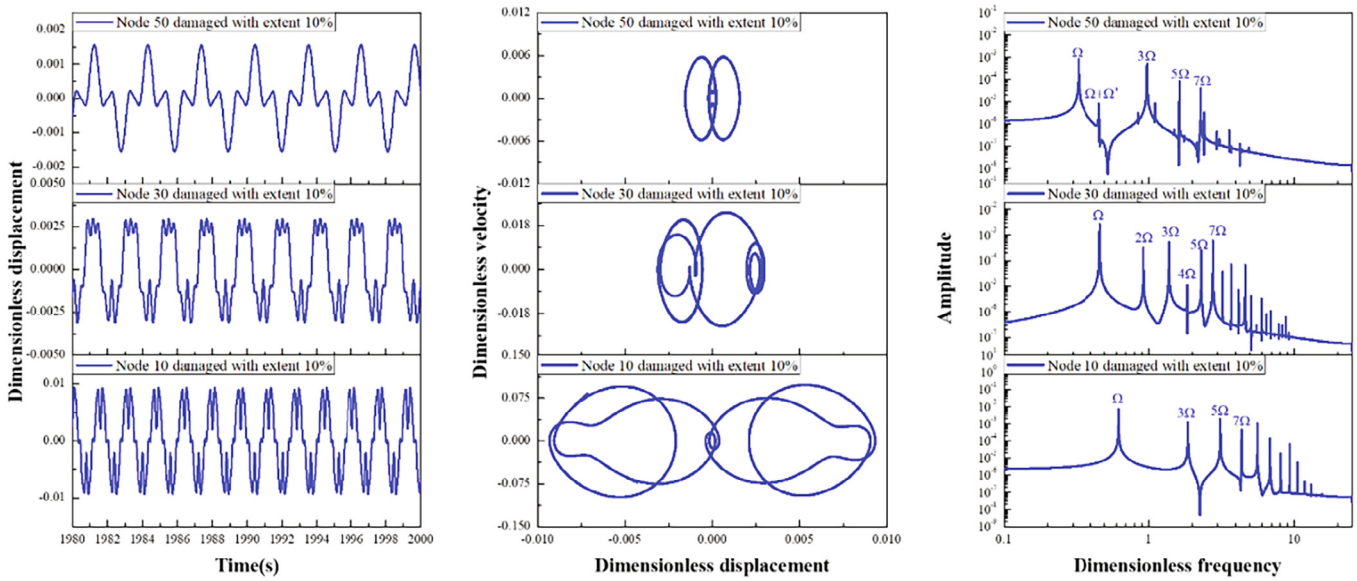

Fig. 11. The comparison of the dimensionless displacements and limit cycles of the node 5 of the tube when the flow pitch velocity is 1.938 m/s.

where η_a is the displacement at $\xi = \xi_a$.

Notice that the coupling term is the impact force between the tube and tube support plate $f^*(\eta_a)$ due to the constraint at the loose support, which can be calculated from the mathematical model presented by Paidoussis *et al.* (Païdoussis et al., 1989; Païdoussis and Li, 1992) as follows:

$$f^*(\eta_a) = \kappa \eta_a^3 \tag{15}$$

where κ is the nondimensional stiffness of the cubic spring. In this paper, κ is chosen to be 1000 in accordance with reference.

3. Dynamic responses of cracked tube subject to cross-flow and loose support

In this section, we take a tube damaged at node 10 with extent 10% as an example to study the dynamic responses of the cracked tube subject to cross-flow and loose support for three flow pitch velocity conditions (U_p = 1.476 m/s, U_p = 1.938 m/s, and U_p = 2.399 m/s, respectively). According to the dynamic model of tube with a crack subject to cross-flow and loose support presented above, the finite difference solution was adopted to divide the cracked tube into 59 elements with 60 nodes. Then, using a fourth-order Runge-Kutta integration algorithm, the nonlinear dynamic responses of a tube damaged at node 10 with extent 10% when the flow pitch velocity is 1.476 m/s, 1.938 m/s, and 2.399 m/s were calculated, respectively. To investigate the effects of the crack on the dynamic characteristics of the tube subjected to cross-flow and loose support more detailly, a comparison between the intact tube and the cracked tube was made. The RMS (root-mean-square) of the dimensionless displacements of the intact and cracked tube when the flow pitch velocity is 1.476 m/s, 1.938 m/s, and 2.399 m/s were illustrated in Fig. 2(a)–(c), separately. (When the flow pitch velocity is 1.476 m/s, 1.938 m/s, and 2.399 m/s, the RMS (root-mean-square) of the

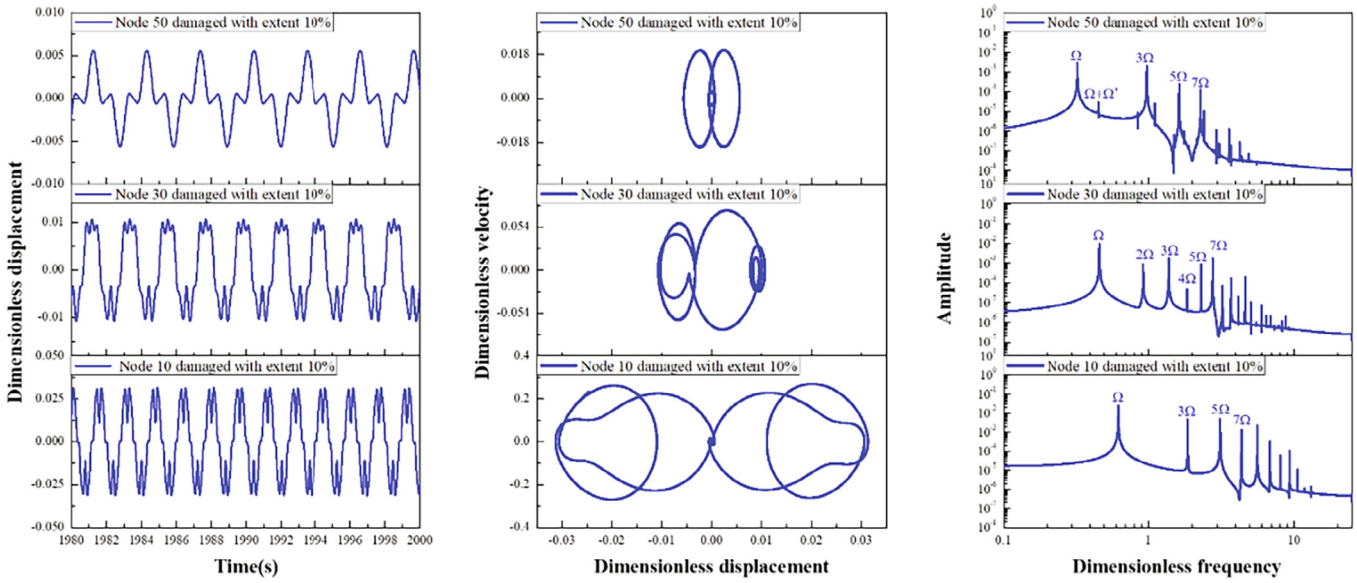

Fig. 12. The comparison of the dimensionless displacements and limit cycles of the node 10 of the tube when the flow pitch velocity is 1.938 m/s.

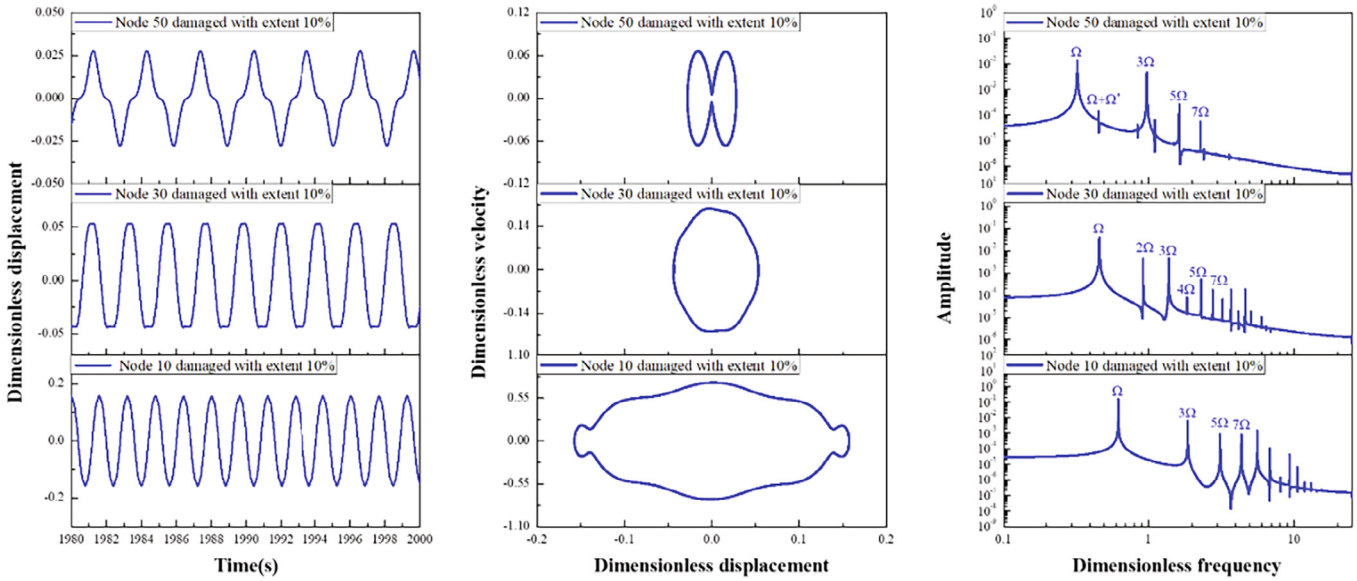

Fig. 13. The comparison of the dimensionless displacements and limit cycles of the node 30 of the tube when the flow pitch velocity is 1.938 m/s.

dimensionless displacements of the intact and cracked tube were illustrated in Fig. 2(a)–(c).) It can be clearly seen that when the flow pitch velocity is 1.476 m/s, the difference between the RMS of the dimensionless displacements of the intact and cracked tube is generally small. With the increasing of the flow pitch velocity, the influences of the crack on the RMS dimensionless displacements of the tube are significantly increased. It is interesting to note that for the high flow pitch velocity conditions, such as the example considered in this study, U_p = 1.938 m/s and U_p = 2.399 m/s, the dynamic characteristics of the cracked tube are different from those of the intact tube. In other word, the damage of the tube may change the mode of the vibration. When the flow pitch velocity is 1.476 m/s, the tube support plates do not provide effective supports, the 1st flexural vibration mode of a cantilever beam can be observed in Fig. 2(a). This type of mode can be called "support-inactive". With increasing of the flow pitch velocity, the cracked tube responds as a cantilever beam supported by the tube support plate, the 2nd flexural vibration mode has been observed, which can be called "support-active", as shown in Fig. 2(b)–(c), while the vibration modes of the intact tube are still support-inactive mode. It is also important to note that, for the damaged tube, the higher vibration mode of the tube may become instability firstly than the fundamental vibration mode, which is different from the phenomenon of the undamaged tube observed in our previous studies.

As shown in Fig. 2, the dynamic responses of the different nodes of the tube are quite different. Thus, to further study the influences of the dynamic characteristics of the cracked tube, four nodes of the tube are chosen from the clamped end to the free end in the comparison in this study, which are node 5, node 10, node 30, and node 60. To have a clear picture of the dynamics of the intact and cracked tube, the time histories of the dimensionless displacement, limit cycles, and dimensionless frequency spectra of the four nodes of intact and cracked tube when the flow pitch velocity is

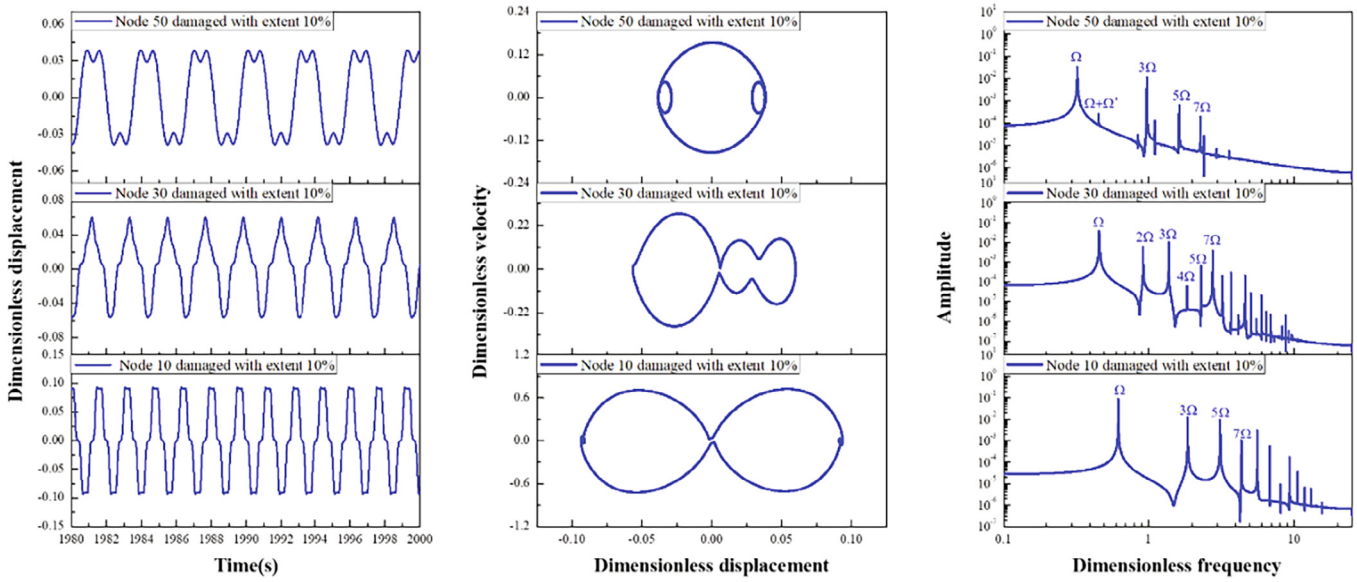

Fig. 14. The comparison of the dimensionless displacements and limit cycles of the node 60 of the tube when the flow pitch velocity is 1.938 m/s.

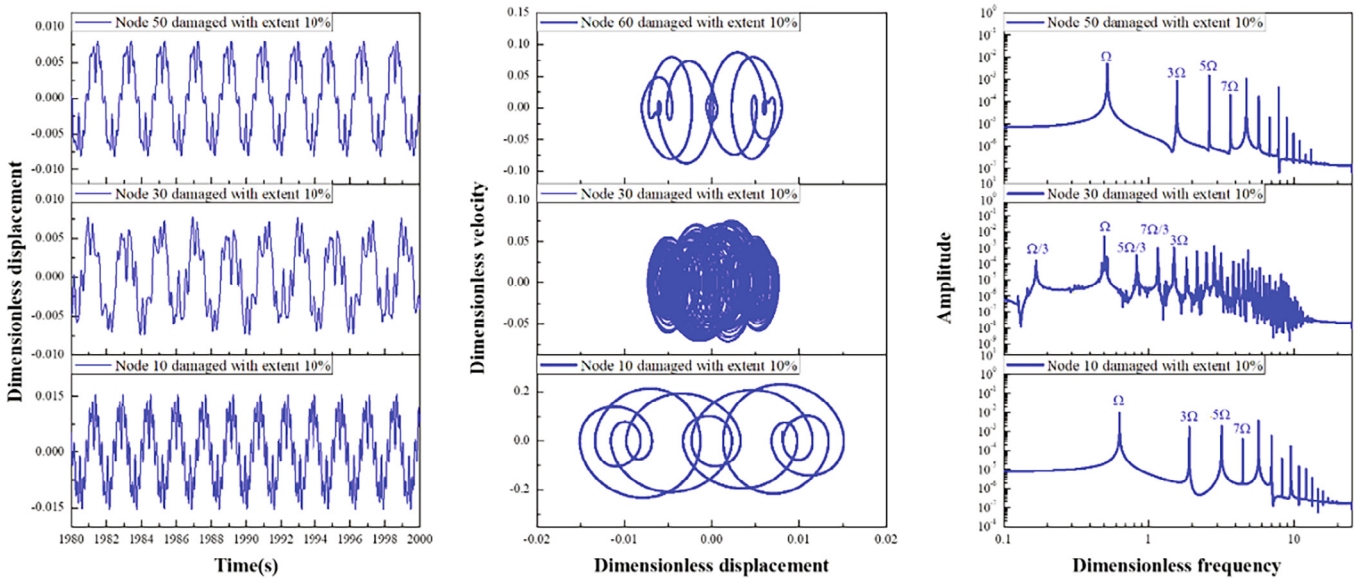

Fig. 15. The comparison of the dimensionless displacements and limit cycles of the node 5 of the tube when the flow pitch velocity is 2.399 m/s.

1.476 m/s were illustrated in Fig. 3(a)–(l), respectively. It can be obviously seen from Fig. 3 that the vibration amplitudes of the four nodes of the cracked tube are equal to those of the intact tube when the flow pitch velocity is 1.476 m/s. The periodic motions of the intact and cracked tubes can also be observed and the trajectories of the four nodes are all toward stable limit cycles. Moreover, with the effects of the loose support, the fundamental frequency of the periodic motion for the cracked tube is larger than the fundamental frequency for the intact tube, and when the periodic motion occurs, the odd frequencies appear in addition to the fundamental frequency, Ω and Ω', for both intact and cracked tubes at U_p = 1.476 m/s, as shown in Fig. 3(c)(f)(i)(l). In addition, it is also important to note that the dynamic characteristics of the left part of the cracked tube are much more different from those of the right part. The high frequency vibrations of the left part of the cracked tube (node 5 and node 10), such as 11 Ω and 13 Ω, can be observed. Furthermore, the vibration of the cracked tube at node 60 is much more complicated as shown in Fig. 3(j), possibly indicating that the collision behavior, such as the collision force and collision frequency, between the tube and loose support, such as anti-vibration bar and tube support plate, may be affected by the crack. It can be clearly seen in Fig. 3(j) that, during one oscillation cycle, one collision between the tube without damage and loose support occurred, while for the cracked tube, there was not just one collision, but two.

The time histories of the dimensionless displacement, limit cycles, and dimensionless frequency spectra of the four nodes of intact and cracked tube when the flow pitch velocity is 1.938 m/s were illustrated in Fig. 4(a)–(l), respectively. As mentioned above, when the flow pitch velocity increases to 1.938 m/s, the vibration

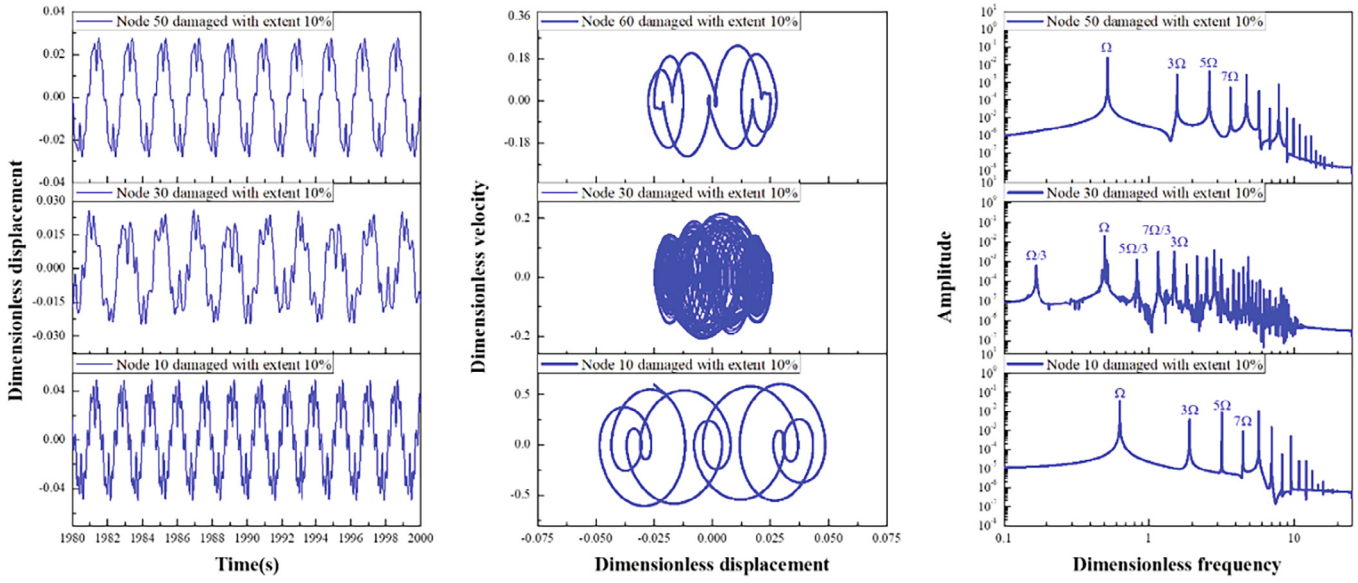

Fig. 16. The comparison of the dimensionless displacements and limit cycles of the node 10 of the tube when the flow pitch velocity is 2.399 m/s.

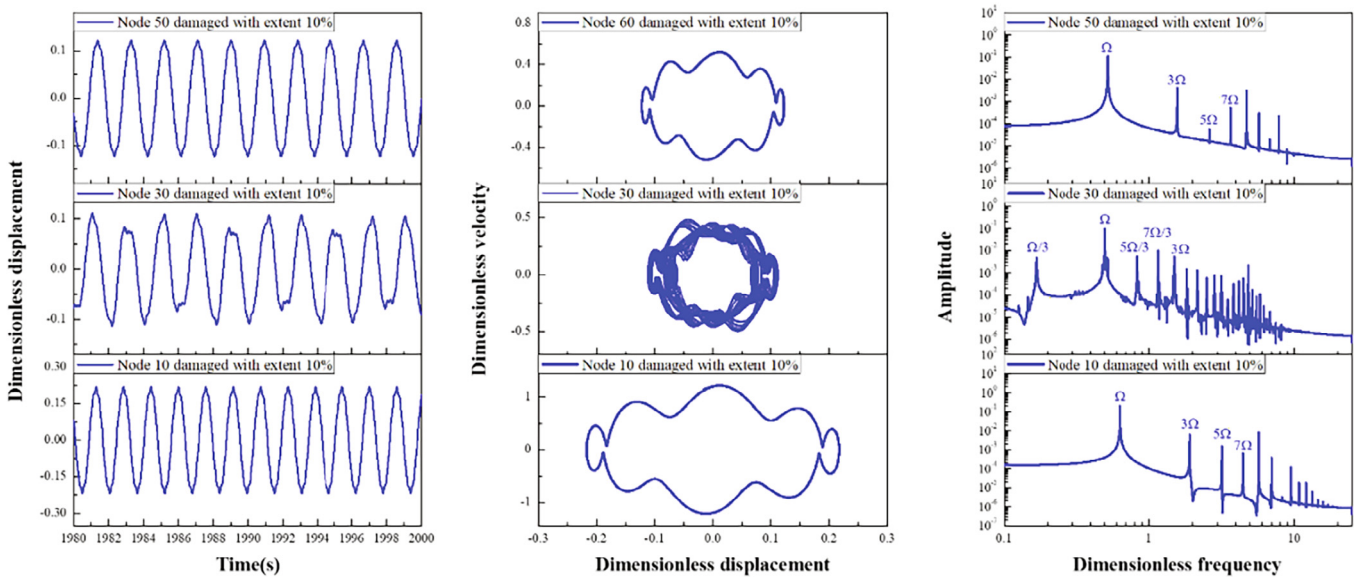

Fig. 17. The comparison of the dimensionless displacements and limit cycles of the node 30 of the tube when the flow pitch velocity is 2.399 m/s.

mode of the cracked tube changes into the support-active mode, the vibration amplitudes of the tube with damage become much larger than those of the intact tube. And, the limit cycle motions of the cracked tube are much more complicated, especially for the left part of the cracked tube. With increasing of the flow pitch velocity, the effects of the loose support on both the fundamental frequency and high frequency of the cracked tube become more visible than those of the intact tube, as shown in Fig. 4(c), (f), (i) and (l). The high order vibration frequency vibrations of the cracked tube, such as 11 Ω, 13 Ω, 15 Ω and 17 Ω, can be observed for both the left and right part of the cracked tube. It can be seen from Fig. 4(j) that the collision behaviors of the intact and cracked tube at U_p = 1.938 m/s are also more complicated than those at U_p = 1.476 m/s. For the intact tube, during one oscillation cycle, two impacts between the tube and support structure take place. For the cracked tube, the typical impact and sliding behavior can be observed, which may cause more serious damage of the fretting-wear due to the tube vibration.

The time histories of the dimensionless displacement, limit cycles, and dimensionless frequency spectra of the four nodes of intact and cracked tube when the flow pitch velocity is 2.399 m/s were illustrated in Fig. 5(a)–(l), respectively. It can be clearly seen that when the flow pitch velocity increases to 2.399 m/s, the vibration amplitudes of the tube with damage are also larger than those of the intact tube. The trajectory of the cracked tube is toward a stable limit cycle, the odd frequency can also be observed besides the fundamental frequency. However, the limit cycle motions of the intact tube are much more complicated than those of the cracked tube. It is important to note that the dimensionless frequency spectrum of the intact tube has peaks at Ω-Ω', Ω-2 Ω', Ω, Ω+Ω', Ω+2 Ω', Ω+3 Ω', *et al.* as shown in Fig. 5(c)(f)(i)(l). Besides, the odd frequency and high frequency can also be observed. In addition, the collision behavior of the cracked tube becomes much more complicated, several impacts between the tube and support structure occur, during one oscillation cycle, as shown in Fig. 5(j).

4. The influence of the crack position on tube dynamic responses

In this section, the influences of the crack position on the tube dynamic responses have been investigated in three cases (case 1: tube damaged at node 10 with extent 10%, case 2: tube damaged at node 30 with extent 10%, and case 3: tube damaged at note 50 with extent 10%, respectively). Each calculation was conducted for the three flow pitch velocity conditions, as in preceding sections.

The RMS of the dimensionless displacements of the three cracked tubes when the flow pitch velocity is 1.476 m/s, 1.938 m/s, and 2.399 m/s were illustrated in Fig. 6(a)–(c), individually. It is obvious that the vibration mode of the three cracked tubes is support-inactive mode at U_p = 1.476 m/s, as shown in Fig. 6(a). With the increasing of the flow pitch velocity, the influences of the position of the damage on the RMS dimensionless displacements of the tube are significantly increased. It should be noted that when the flow pitch velocity is 1.938 m/s, the vibration modes of the tube damaged at note 10 and the tube damaged at note 30 have changed to the support-active mode, while the vibration mode of the tube damaged at note 50 is still the support-inactive mode. For the higher flow pitch velocity, such as the example considered in this study, U_p = 2.399 m/s, the vibration mode of the tube damaged at node 50 also changed to the support-active mode.

Similarly, to further investigate the effects of the position of the damage on the dynamic characteristics of the cracked tube, four nodes of the tube are chosen from the clamped end to the free end in the comparison in this study, which are node 5, node 10, node 30, and node 60. The time histories of the dimensionless displacement, limit cycles, and dimensionless frequency spectra of the four nodes of the three cracked tube when the flow pitch velocity is 1.476 m/s were illustrated in Figs. 7–10, respectively. It can be clearly seen that the position of the damage has a smaller effect on the dynamic responses and limit cycles of the node 5, node 10, and node 30 at U_p = 1.476 m/s. Nevertheless, the dynamic responses, limit cycle motions, and dimensionless frequency spectra of the node 60 of the three cracked tubes are obvious different. For the tube damaged at node 10 with extent 10% two impacts between the tube and support structure take place. And, for the tubes damaged at node 30 and 50 with extent 10%, the impact and sliding behavior occurs.

The time histories of the dimensionless displacement, limit cycles, and dimensionless frequency spectra of the four nodes of the three cracked tube when the flow pitch velocity is 1.938 m/s were illustrated in Figs. 11–14, respectively. With increasing of

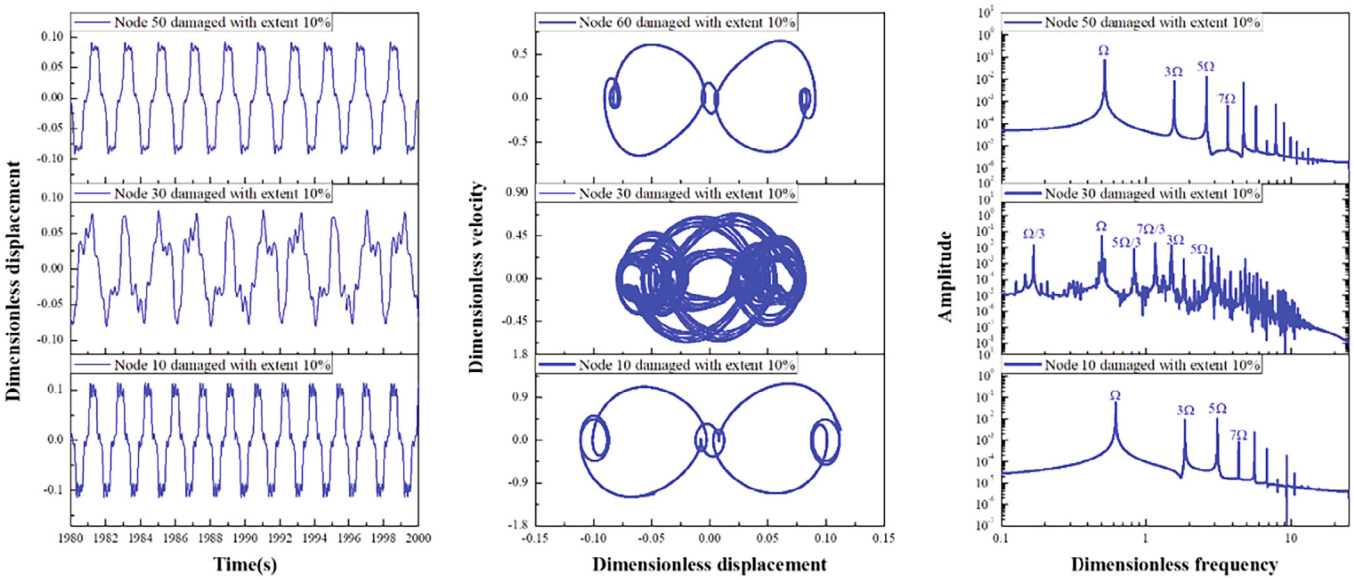

Fig. 18. The comparison of the dimensionless displacements and limit cycles of the node 60 of the tube when the flow pitch velocity is 2.399 m/s.

the flow pitch velocity, the high-frequency vibrations of the cracked tubes become obviously, and the vibrations of the cracked tubes are much more complicated than those of the cracked tubes at U_p = 1.476 m/s. It is interesting to note that, for the tube damaged at node 10, besides the fundamental frequency the odd frequency can be observed. For the tube damaged at node 30, both the even and odd frequency can be observed. For the tube damaged at node 50, the dimensionless frequency spectrum has a peak at Ω +Ω', besides the odd frequency and high frequency.

The time histories of the dimensionless displacement, limit cycles, and dimensionless frequency spectra of the four nodes of the three cracked tube when the flow pitch velocity is 2.399 m/s were illustrated in Figs. 15–18, respectively. It is important to note that at U_p = 2.399 m/s the quasi-periodic motion of the tube damaged at node 30 with extent 10% occurs, and the dimensionless frequency spectrum has peaks at Ω/3, 5 Ω/3, and 7 Ω/3, besides the odd frequency and high frequency, which is different from the phenomenon observed in other cases. For the tube damaged at node 10 and node 50 with extent 10%, the periodic motions can also be observed and the trajectories of the four nodes are all toward stable limit cycles.

5. Conclusion

The dynamic characteristics of a flexible tube with a crack in a rotated triangular tube array considering the effects of cross-flow and loose support were investigated by building a mathematical model in present study. The model takes into account the variations of the tube natural frequency and mode of vibration owing to the crack damage. To analyze the effect of the crack damage on the dynamic characteristics of a flexible tube in tube bundles subject to cross-flow and loose support, the dynamic responses of the cracked tube were calculated for three flow pitch velocity conditions. From these analyses, we have drawn the following conclusions:

1. For all the flow pitch velocity conditions concerned in this study, the crack damage can change the vibration characteristics of the tube. For the intact tube, the tube support plates do not provide effective supports, called as "support inactive", at the three flow pitch velocity conditions concerned in present study. For the cracked tube, the support inactive vibration mode also be observed at U_p = 1.476 m/s. With increasing of the flow pitch velocity, the vibration mode of the cracked tube, called as "support active", was observed, which is different from the phenomenon of the undamaged tube.
2. The limit cycle motions of the cracked tube are much more complicated. As the flow pitch velocity increases, the effects of the loose support on both the fundamental frequency and high frequency of the cracked tube become more visible than those of the intact tube.
3. The collision behavior of the cracked tube becomes much more complicated, the impact-sliding and several impacts between the tube and support structure occur, during one oscillation cycle, which may cause more serious damage of the fretting-wear due to the tube vibration.
4. The influences of the crack position on the dynamic characteristics of the tube are significant. For the tube damaged at node 10 and node 50 with extent 10%, the periodic motions were observed for the three flow pitch velocity conditions. While for the tube damaged at node 30 with extent 10%, the quasi-periodic motion of the cracked tube occurs at U_p = 2.399 m/s.

CRediT authorship contribution statement

Jiang Lai: Conceptualization, Funding acquisition, Methodolgy, writing-review & editing. **Lingling Lu:** Methodology, Funding acquisition, Visualization, Validation. **Shihao Yang:** Investigation. **Tiancai Tan:** Writing-original draft. **Lei Sun:** Supervision, Project administration.

Declaration of Competing Interest

The authors declare that they have no known competing financial interests or personal relationships that could have appeared to influence the work reported in this paper.

Acknowledgments

This research is supported by the National Natural Science Foundation of China (Grant Nos. 12072336) and State Key Labora-

tory of Hydraulic Engineering Simulation and Safety (Tianjin University) (Grant Nos. HESS-2107).

References

Austermann, R., Popp, K., 1995. Stability behavior of a single flexible cylinder in rigid tube arrays of different geometry subjected to cross-flow. J. Fluids Struct. 9, 303–322.

Bamnios, G., Trochides, A., 1995. Dynamic behaviour of a cracked cantilever beam. Appl. Acoust. 45 (2), 97–112.

Chati, M., Rand, R., Mukherjee, S., 1997. Modal analysis of a cracked beam. J. Sound Vib. 207 (2), 249–270.

Chen, S.S., Srikantiah, G.S., 2001. Motion-dependent fluid force coefficients for tube arrays in crossflow. J. Pressure Vessel Technol. 123, 429–436.

de Pedro Palomar, B., Meskell, C., 2018. Sensitivity of the damping controlled fluidelastic instability threshold to mass ratio, pitch ratio and Reynolds number in normal triangular arrays. Nucl. Eng. Des. 331, 32–40.

Hassan, M., Hayder, M., 2008. Modelling of fluidelastic vibrations of heat exchanger tubes with loose supports. Nucl. Eng. Des. 238 (10), 2507–2520.

Lai, J., 2019. Analysis on streamwise fluidelastic instability of rotated triangular tube arrays subjected to two-phase flow. Mech. Syst. Sig. Process. 123, 192–205.

Lai, J., Sun, L., Li, P., 2019. Two-phase flow-induced instability and nonlinear dynamics of a single tube in tube bundles in the transverse direction. European Journal of Mechanics / A Solids 78, 103858. https://doi.org/10.1016/j.euromechsol.2019.103858.

Lai, J., Sun, L., Li, P., Tan, T., Gao, L., Xi, Z., He, C., Liu, H., 2019. Eigenvalue analysis on fluidelastic instability of a rotated triangular tube array considering the effects of two-phase flow. J. Sound Vib. 439, 194–207.

Lai, J., Sun, L., Gao, L., Tan, T., Xi, Z., Li, P., 2019. Study on fluidelastic instability of a tube array subjected to two-phase cross-flow. Ann. Nucl. Energy 126, 303–311.

Lai, J., He, C., Sun, L., Tan, T., 2020. Theoretical and experimental study on the fluidelastic instability of tube bundles in two-phase cross flow. Int. J. Press. Vessels Pip. 181, 104069. https://doi.org/10.1016/j.ijpvp.2020.104069.

Lai, J., Wu, H., Sun, L., Gao, L., Li, P., 2020. Numerical investigation on Hopf bifurcation and post-instability of tube bundles subjected to two-phase cross-flow and loose support. Ann. Nucl. Energy 143, 107459. https://doi.org/10.1016/j.anucene.2020.107459.

Lai, J., Sun, L., Gao, L., Li, P., Tan, T., 2020. Theoretical investigation of fluidelastic instability of a rotated triangular tube array in two-phase flow. Arch. Appl. Mech. 90 (10), 2347–2362. https://doi.org/10.1007/s00419-020-01725-z.

Lai, J., Sun, L., Gao, L., Tan, T., Li, P., 2020. Two-phase flow-induced instability and nonlinear dynamics of a rotated triangular tube array in parallel direction. Eur. J. Mech. / Solids 83, 104024. https://doi.org/10.1016/j.euromechsol.2020.104024.

Li, H., Mureithi, N., 2017. Development of a time delay formulation for fluidelastic instability model. J. Fluids Struct. 70, 346–359.

Ostachowicz, W.M., Krawczuk, M., 1991. Analysis of the effect of cracks on the natural frequencies of a cantilever beam. J. Sound Vib. 150 (2), 191–201.

Païdoussis, M.P., Li, G.X., Moon, F.C., 1989. Chaotic oscillations of the autonomous system of a constrained pipe conveying fluid. J. Sound Vib. 135 (1), 1–19.

Païdoussis, M.P., Li, G.X., 1992. Cross-flow-induced chaotic vibrations of heat-exchanger tubes impacting on loose supports. J. Sound Vib. 152 (2), 305–326.

Piteau, P., Delaune, X., Borsoi, L., Antunes, J., 2019. Experimental identification of the fluid-elastic coupling forces on a flexible tube within a rigid square bundle subjected to single-phase cross-flow. J. Fluids Struct. 86, 156–169.

Sadek, O., Mohany, A., Hassan, M., 2018. Numerical investigation of the cross flow fluidelastic forces of two-phase flow in tube bundles. J. Fluids Struct. 79, 171–186.

Sawadogo, T., Mureithi, N., 2014. Fluidelastic instability study on a rotated triangular tube array subject to two-phase cross-flow. Part I: Fluid force measurements and time delay extraction. J. Fluids Struct. 49, 1–15.

Tanaka, H., Takahara, S., 1981. Fluid elastic instability of tube array in cross flow. J. Sound Vib. 77 (1), 19–37.

Wang, L., Ni, Q., 2010. Hopf bifurcation and chaotic motions of a tubular cantilever subject to cross flow and loose support. Nonlinear Dyn. 59 (1-2), 329–338.

Xu, W., Ji, C., Sun, H., Ding, W., Bernitsas, M.M., 2019. Flow-induced vibration of two elastically mounted tandem cylinders in cross-flow at subcritical numbers. Ocean Eng. 173, 375–387.

Zhang, X.u., Jiang, B., Zhang, L., Xiao, X., 2016. Fluid-elastic instability tests on parallel triangular tube bundles with different mass ratio values under increasing and decreasing flow velocities. Shock Vib. 2016, 1–20.

Zhao, W., Xue, F., Shu, G., Liu, M., Lin, L., Wang, Z., Xiao, Z., 2014. Analysis of flow-induced vibration of steam generator tubes subjected to cross flow. Nucl. Eng. Des. 275, 375–381.